Draft version November 15, 2011
Preprint typeset using LaTeX style emulateapj v. 6/22/04

UNUSUAL CENTRAL ENGINE ACTIVITY IN THE DOUBLE BURST GRB 110709B

Bin-Bin Zhang[1], David N. Burrows[1], Bing Zhang[2], Peter Meszaros[1,3], Giulia Stratta[4,5], Valerio D'Elia[4,5], Dmitry Frederiks[6], S. Golenetskii[6], Jay R. Cummings[7,8], Xiang-Yu Wang[9,10], Abraham D. Falcone[1], Scott D. Barthelmy[11], Neil Gehrels[11]

Draft version November 15, 2011

ABSTRACT

The double burst, GRB 110709B, triggered *Swift*/BAT twice at 21:32:39 UT and 21:43:45 UT, respectively, on 9 July 2011. This is the first time we observed a GRB with two BAT triggers. In this paper, we present simultaneous *Swift* and Konus-*WIND* observations of this unusual GRB and its afterglow. If the two events are from the same physical origin, their different time-dependent spectral evolution suggest they must belong to different episodes of the central engine, which may be a magnetar-to-BH accretion system.

Subject headings: gamma-ray burst: general

1. INTRODUCTION

Gamma-Ray Bursts (GRBs) have been thought to be one-time events through both observation and theoretical understanding. The general picture of a GRB is as follows: (1) A "central engine" consisting of a rapidly rotating black hole (BH) and a nuclear-density accretion disk is formed from a progenitor system, which invokes either core-collapse of a massive star (Woosley 1993; MacFadyen & Woosley 1999, Fryer et al 2007) or merger of two compact stellar objects such as NS-NS or BH-NS (Paczýnski 1986; Eichler et al. 1989; Paczýnski 1991; Narayan et al. 1992). (2) A relativistically expanding ejecta, which is composed of many mini-shells with a wide-range of Lorentz factors, is launched by the central engine. Internal shocks (Rees & Mészáros 1994) are formed during the collisions of those shells and produce the observed prompt GRB emission (mostly in Gamma-ray band). Observationally this is the phase when GRBs trigger gamma-ray band detectors. (3) The ejecta are further decelerated by an ambient medium (e.g, interstellar medium; ISM) and produce a long-term broad band afterglow through an external-forward shock (Mészáros & Rees 1997a; Sari et al. 1998) and/or external-reverse shock (Mészáros & Rees 1997a, 1999; Sari & Piran 1999a,b). (4) In some cases, the central engine can be restarted during the afterglow phase and X-ray flares are produced through dissipation of a late wind launched from a long-lasting central engine (Burrows et al. 2005b; Zhang et al. 2006; Fan & Wei 2005; Ioka et al. 2005; Wu et al. 2005; Falcone et al. 2006; Romano et al. 2006; Lazzati & Perna 2007; see Zhang 2007 for review). Although X-ray flares are generally regarded to have the same physical origin as prompt emission, they release their energy mostly in the soft X-ray band.

GRB 110709B triggered the Burst Alert Telescope (BAT; Barthelmy et al. 2005) on-board *Swift* twice. Each of the triggers, separated by 11 minutes, consists of an otherwise typical long GRB light curve in the hard X-ray/gamma-ray band. X-ray observations during the second burst show that this event also produced bright soft X-ray emission. This provides a rare opportunity to conduct a detailed broad-band study of the central engine properties.

In this paper, we first report the *Swift* and Konus-*WIND* observations of GRB 110709B in §2. Then we present multi-wavelength spectroscopy and timing studies in §3. The physical implications on the central engine properties are discussed in §4. We draw our conclusions in §5.

2. OBSERVATIONS AND DATA ANALYSIS

2.1. *Swift Data*

GRB 110709B first triggered the Burst Alert Telescope (BAT; Barthlmy et al. 2005) on-board *Swift* at 21:32:39 UT on 9 July 2011 (Cummings et al 2011a). *Swift* slewed immediately to the burst. The two narrow field instruments, the X-ray Telescope (XRT; Burrows et al. 2005a) and the Ultraviolet Optical telescope (UVOT; Roming et al. 2005) on-board *Swift* began to observe the field at $T_0 + 80.5$ seconds and $T_0 + 91$ seconds, respectively, where T_0 is the BAT trigger time. A bright X-ray afterglow was localized at R.A.(J2000) = $10^h58^m37.08^s$, Dec.(J2000) = $-23°27'17''.6$ with an uncertainty of $1''.4$ (90% confidence, Beardmore et al. 2011). No reliable optical source was found within the XRT error circle (Holland et al 2011a,b).

Interestingly, at 21:43:25 UT on 9 July 2011, 11 minutes after the first trigger, the BAT was triggered again

[1] Department of Astronomy and Astrophysics, Pennsylvania State University, University Park, PA 16802, USA; bbzhang@psu.edu
[2] Department of Physics, University of Nevada, Las Vegas, NV 89154, USA
[3] Department of Physics, Pennsylvania State University, University Park, PA 16802, USA
[4] ASI-Science Data Center, Via Galileo Galilei, I-00044 Frascati, Italy
[5] INAF-Osservatorio Astronomico di Roma, Via Frascati 33, I-00040 Monteporzio Catone, Italy
[6] Ioffe Physico-Technical Institute, Laboratory for Experimental Astrophysics, 26 Polytekhnicheskaya, St Petersburg 194021, Russian Federation
[7] CRESST and NASA/GSFC, Greenbelt, MD 20771, USA
[8] University of Maryland, Baltimore County, 1000 Hilltop Circle, Baltimore, MD 21250, USA
[9] Department of Astronomy, Nanjing University, Nanjing, 210093, China
[10] Key laboratory of Modern Astronomy and Astrophysics (Nanjing University), Ministry of Education, Nanjing 210093, China
[11] NASA Goddard Space Flight Center, Greenbelt, MD 20771, USA

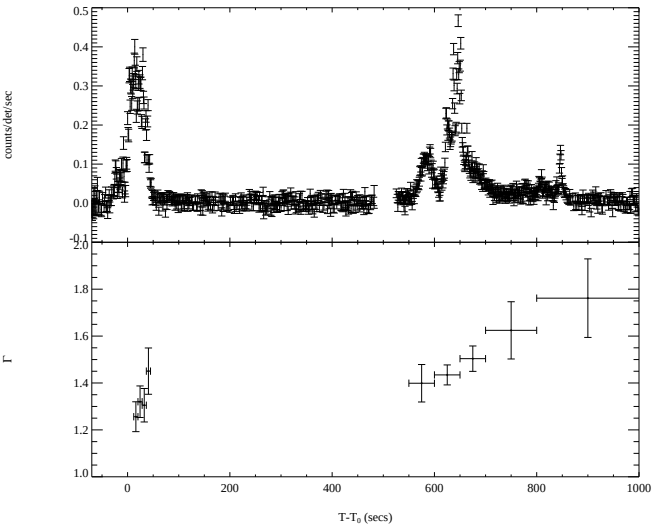

FIG. 1.— BAT count rates (upper panel) and photon index evolution (lower panel) of GRB 110709B. The spectral model is a simple power law.

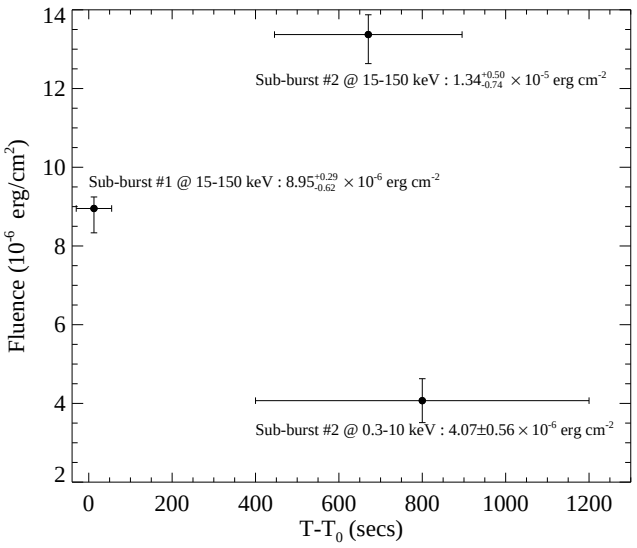

FIG. 2.— Comparison between the fluences of the first sub-burst (15-150 keV) and the second sub-burst (0.3-10 keV and 15-150 keV).

and located a second event from the same location (Barthelmy et al 2011). The second outburst has comparable intensity and light curve characteristics to the first outburst. Regarding the two outbursts as two episodes of a single burst, the separation (11 minutes) is the longest compared to other multi-episode bursts. In this paper, we use the term "double burst" to stress the unusual nature of this double-trigger GRB. We will use the term "the first sub-burst" to refer to the first outburst and "the second sub-burst" to refer to the second outburst. However, as we will show below, the two events are clearly related, indicating that they have the same physical origin.

We processed the *Swift*/BAT data using standard HEAsoft tools (version 6.11). As shown in Fig. 1, the first sub-burst lasted from T_0-28 seconds to T_0+55 seconds with $T_{90,1st} = 55.6 \pm 3.2$ seconds. The second sub-burst lasted from $\sim T_0 + 550$ seconds to about $T_0 + 865$ seconds with $T_{90,2nd} = 259.2 \pm 8.8$ seconds (Cummings et al 2011b). There was no flux detectable in BAT from about $T_0 + 180$ seconds to about $T_0 + 550$ seconds. We extracted the BAT spectra in several slices. The lower panel in Fig. 1 shows the photon indices obtained by fitting the spectra with a simple power-law model. It is obvious that both sub-bursts have strong hard-to-soft spectral evolution. The photon indices range from ~ 1.25 to ~ 1.75. The BAT band (15-150 keV) fluences of the first and second sub-bursts are $8.95^{+0.29}_{-0.62} \times 10^{-6}$ erg cm^{-2} and $1.34^{+0.50}_{-0.74} \times 10^{-5}$ erg cm^{-2} respectively (see Fig. 2).

We processed the *Swift*/XRT data using our own IDL codes which employ the standard HEAsoft analysis tools. For technical details please refer to Zhang et al 2007. Fig. 3 shows the XRT light curve and spectral evolution. The prolonged and energetic flaring activity continues up to $T_0 + 2000$ seconds, which corresponds to the second sub-burst time period. The light curve after the flare can be fitted by a broken power-law with $\alpha_1 = 0.98 \pm 0.08$, $\alpha_2 = 1.6 \pm 0.13$ and a break time $t_b = 5.9 \pm 4.1 \times 10^4$ s. The X-ray spectrum can be fitted with an absorbed power-law with total column $N_H = 2.14^{+0.22}_{-0.21} \times 10^{21}$cm^{-2} which includes the Galactic foreground $N_H = 5.6 \times 10^{20}$cm^{-2} (D'Elia et al 2011). Strong spectral evolution was observed in the flare phase where the photon indices vary significantly from $\Gamma \sim 0.9$ to $\Gamma \sim 2.6$. The late time spectrum has no significant evolution with an average photon index $\Gamma \sim 2.1$. The total fluence in XRT band (0.3-10 keV) is $4.07 \pm 0.56 \times 10^{-6}$ erg cm^{-2} (see Fig. 2).

In order to check whether the break in XRT light curve is due to curvature caused by an incorrect reference time T_0 effect (e.g., Yamazaki 2009 and Liang et al. 2009, 2010), we plot the XRT light curve in reference to the trigger time of the second sub-burst. We find that the t_b, α_1 and α_2 do not significantly change within 1-sigma range. We thus conclude that the break is intrinsic.

2.2. *A Lensed Burst?*

The similarity of the two sub-bursts raises the question of whether they could be produced by gravitational lensing of a single GRB located behind a foreground galaxy. To investigate this possibility, we examined Chandra observations of GRB 110709B at 14:15:04 UT on 23 July 2011 (day 14; 15.05 ks exposure time; Observation ID 12921) and at 19:50:34 UT on 31 October 2011 (day 114; 10 ks exposure time; Observation ID 14237). We downloaded the public Chandra data from the Chandra archive[12] and processed them using the standard CIAO tools (version 4.3). The first Chandra observation has two X-ray point sources in the field of GRB 110709B, with nearly identical brightness (3.7×10^{-3} s^{-1}, 0.2-8 keV) and separated by only 3.4 arcseconds (Fig. 4). Source 1 is located 0.67 arcseconds from the

[12] `http://cda.harvard.edu/chaser`

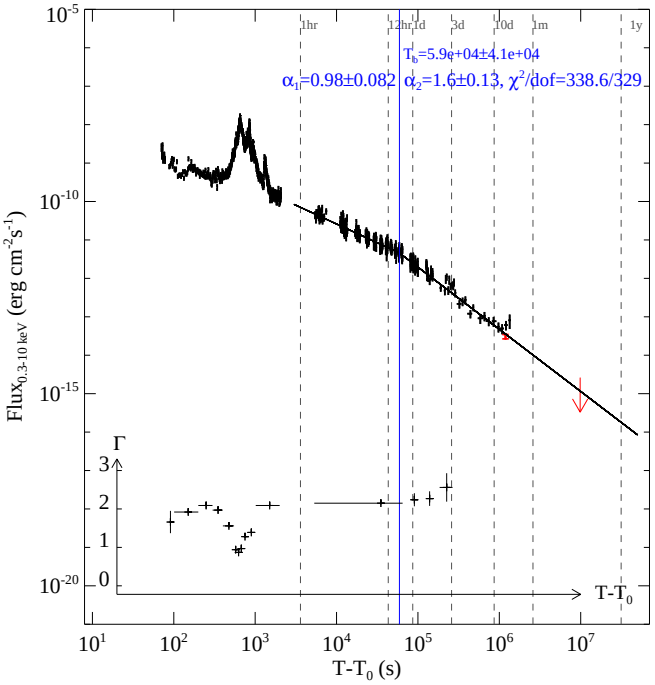

FIG. 3.— *Swift*/XRT light curve of GRB 110709B. Inner plot shows the photon index evolution. Red points are from Chandra observations (see §3.4). The solid line shows the broken power-law fit to the lightcurve after the flare.

refined XRT position, within the refined XRT error circle. Both sources are within the XRT point-spread function (18 arcseconds Half-Power-Diameter), and the sum of their fluxes is consistent with the total XRT flux measured during the first epoch, while the flux of Source 1 is consistent with the extrapolation of the XRT light curve (Fig. 3). The field was unobservable by both Chandra and Swift from about 8 August 2011 until 28 October 2011. In the second Chandra observation, taken shortly after the field emerged from the Chandra Sun (pitch angle) constraint, Source 1 has vanished, while Source 2 is still present, with a slightly lower count rate of $\sim 2.7 \times 10^{-3}$ s^{-1} (0.2-8 keV), consistent with being a background X-ray source such as an AGN. The upper limit for the Source 1 flux is still consistent with the extrapolation of the XRT light curve (Fig. 3). The fact that Source 1 vanished while Source 2 did not clearly rules out any possibility that the double burst is due to gravitational lensing.

2.3. Konus-*Wind* Data

GRB 110709B triggered detector S1 of the Konus-*WIND* gamma-ray spectrometer (Apterkar et al. 1995) at 21:32:44.567 s UT on 9 July 2011 (Golenetskii et al 2011). Konus-*WIND* recorded the first sub-burst with high-resolution data. The T_{90} of the first sub-burst in Konus-*WIND* energy band (20 keV - 5 MeV) is 51.3 ± 7.6 s. The fluence in the same energy range is $2.6 \pm 0.2 \times 10^{-5}$ erg cm^{-2}. The second sub-burst fell into a telemetry gap but was recorded by the instrument's spare count rate measurement channel (Fig. 5). The overlap detection of the first sub-burst will allow a BAT+Konus-*WIND* multi-wavelength study.

3. MULTI-WAVELENGTH TIMING AND SPECTROSCOPY PROPERTIES

3.1. *Joint Spectral Fit*

As shown in Fig 5, the first sub-burst was simultaneously observed by Konus-*WIND* and *Swift*/BAT, so we are able to perform joint spectral fitting using the spectra of those two instruments. We dvide the time period of the first sub-burst into 5 time slices. The exact time ranges of each slice are listed in Table 1. For the first four slices, the best fit model is a cut-off power-law (CPL, cutoffpl in Xspec 12). For the 5th slice, the best fit model is a simple power-law (PL, powerlaw in Xspec 12). The time-dependent fitting results are presented in Table 1. The time-integrated spectrum (3.594 s to 44.810 s) can also be fitted by a cut-off power-law model with $\alpha = 1.17 \pm 0.04$, $E_p = 311^{+45}_{-38}$ and $\chi^2/\mathrm{dof} = 125/129$ (Fig. 6). The second sub-burst was simultaneously observed by *Swift*/BAT and *Swift*/XRT. Similarly with the first sub-burst, we are able to perform joint spectral fitting using the spectra of those two instruments. We divide the time period of the second sub-burst into 5 slices (listed in Table 1). We fit the spectrum of each slice using absorbed cut-off power-law model. An underlying simple power-law decaying component was also taken into account and subtracted using the same strategy as in Falcone et al 2007. The time-dependent fitting results are presented in Table 1. The time-averaged (550s to 1000 s) BAT+XRT spectra are well fitted by the absorbed cut-off power-law model with $\alpha = 1.12 \pm 0.04$, $E_p = 116^{+9}_{-8}$ and $\chi^2/\mathrm{dof} = 687/679$ (Fig. 7).

The spectral evolution during the whole double burst shows an overall hard-to-soft trend. In Fig. 8, we plot the modeled spectral energy distribution in different time intervals, which demonstrates the intrinsic spectral shape evolution. Fig. 9 & 10 show the evolution of E_p and α respectively. Although strong spectral evolution is exhibited by both sub-bursts, their time-dependent behaviors are very different. For example, as shown in Fig 9, the E_p of the first sub-burst decays to $\propto t^{-0.13}$ while the E_p of the second sub-burst decays to $\propto t^{-1.9}$ (or $\propto t^{-0.31}$ if we shift reference time of the second sub-burst to its trigger time). The different time-dependent spectral of the two sub-bursts may suggest that the two sub-bursts are from different stages of the same central engine (see §4 for more discussions).

3.2. E_p-$E_{\gamma,iso}$ *Relation and Implication for Redshift*

There has been no redshift measurement for GRB 110709B, so the rest-frame peak energy, $E_p/(1+z)$, and the isotropic energy, $E_{\gamma,iso}$, are unknown. On the other hand, one can assume it has a redshift z_x and plot the corresponding $E_p(z_x)$ and $E_{\gamma,iso}(z_x)$ on the $E_p - E_{\gamma,iso}$ (Amati relation; Amati et al 2002) diagram. The well-known Amati relation suggests that most long (or type II; Zhang et al 2009) bursts follow the $E_p \propto E^{1/2}_{\gamma,iso}$ track (Amati et al 2002, Zhang et al 2009). Since GRB 110709B is obviously a long burst (especially with two long sub-bursts), in principal it should fall into the same track as other typical long (type II) bursts. In Fig. 11, we assign GRB 110709B onto the E_p-$E_{\gamma,iso}$ diagram by assuming its redshift is in the range of $z_x = 0.01 - 7$. It is

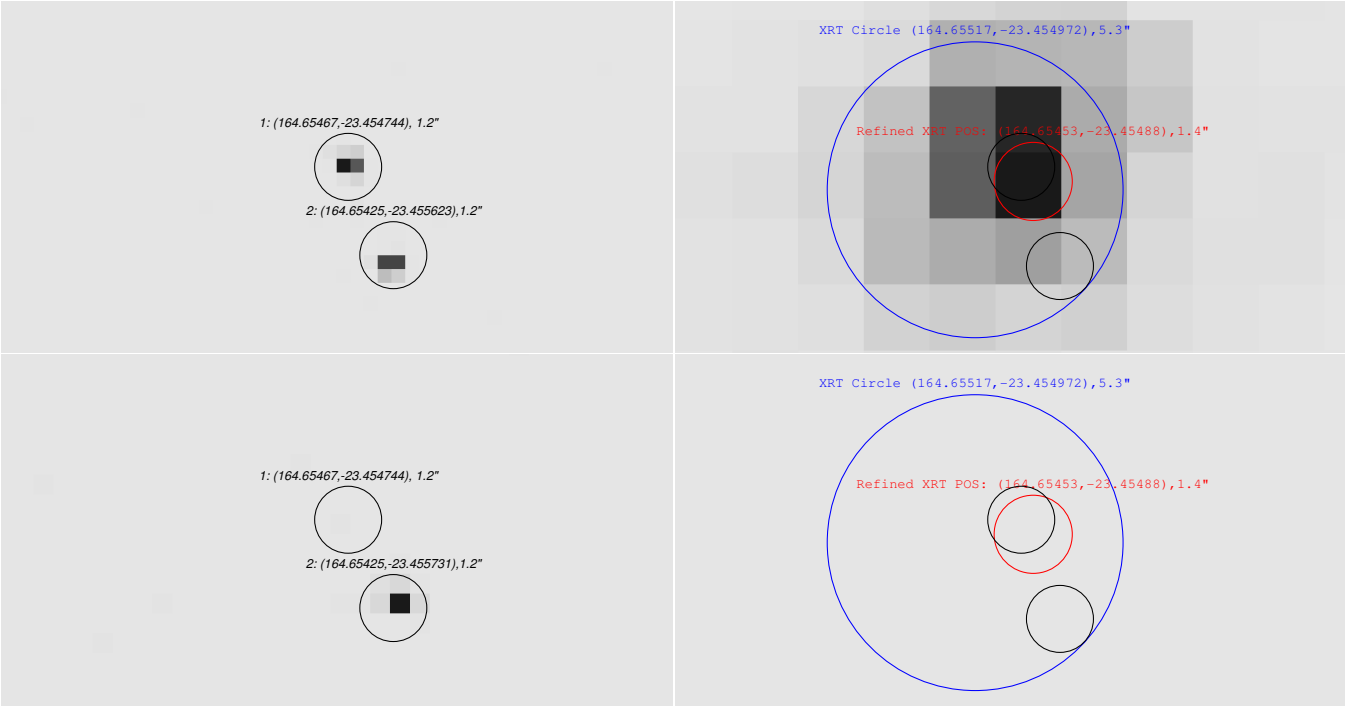

FIG. 4.— *Chandra* (*upper left*: $T_0 + 14$ *days*; *lower left*: $T_0 + 114$ *days*) and *Swift*/XRT (*upper right*: $T_0 + 0$ *day*; *lower right*: $T_0 + 114$ *days*) images of 110709B. Black circles (radius=1.″2) indicate the Chandra source extraction regions at the locations of R.A.(J2000) = $10^h58^m37.121^s$, Dec.(J2000) = $-23°27'17.''08$ and R.A.(J2000) = $10^h58^m37.003^s$, Dec.(J2000) = $-23°27'20.''24$. The red circle is the enhanced XRT error circle (Beardmore et al 2011). The blue circle indicates the preliminary XRT error circle (based on the on-board centroid of the first 2.5 s of data) that was reported by Cummings et al 2011.

TABLE 1
JOINT FIT RESULTS

Time interval s	Model	α	E_p keV	χ^2/dof	Inst.
(3.594,12.042)	CPL	$1.03^a \pm 0.06$	301^{+77}_{-57}	127/128	BAT+KW
(12.042,20.230)	CPL	1.0 ± 0.06	272^{+53}_{-41}	135/128	BAT+KW
(20.230,28.426)	CPL	$1.1^{+0.07}_{-0.06}$	247^{+60}_{-46}	156/128	BAT+KW
(28.426,36.618)	CPL	1.1 ± 0.08	258^{+94}_{-63}	111/128	BAT+KW
(36.618,44.810)	PL	1.55 ± 0.05	–	132/129	BAT+KW
(3.594,44.810)	CPL	1.17 ± 0.04	311^{+45}_{-38}	125/129	BAT+KW
(550,600)	CPL	0.80 ± 0.05	109^{+15}_{-12}	263/303	BAT+XRT
(600,650)	CPL	0.82 ± 0.03	112^{+9}_{-7}	360/418	BAT+XRT
(650,700)	CPL	0.92 ± 0.03	99^{+9}_{-8}	343/365	BAT+XRT
(700,800)	CPL	1.22 ± 0.02	78^{+16}_{-12}	438/456	BAT+XRT
(800,1000)	CPL	1.33 ± 0.02	72^{+17}_{-13}	512/501	BAT+XRT
(550,1000)	CPL	1.12 ± 0.01	116^{+9}_{-8}	687/679	BAT+XRT

[a]Error are given at the 1-sigma level.

interesting to note that, in order to let GRB 110709B fall into the long/Type II track, it apparently should have a redshift of $z_x \geq 0.3$. This may indicate that GRB 110709B is not a nearby event.

3.3. *Spectral Lag*

Spectral lags, which are caused by the fact that softer Gamma-ray photons usually arrive later than hard photons, are always observed in long (type II) GRBs (Norris et al 2000; Gehrels et al . 2006; Liang et al. 2006; Zhang et al 2009), but are typically negligible for short (type I) GRBs (Norris & Bonnell 2006; Zhang et al 2009). For the first sub-burst, we extracted 64ms-binned light curves in the following four BAT energy bands: 15−25 keV, 25−50 keV, 50 − 100 keV and 100 − 150 keV and the following three Konus-*WIND* bands: 25−95 keV, 95−380 keV and 380 − 1435 keV. Then, using the CCF (cross-correlation function; Norris et al 2000) method, we calculate the lags between any two light curves in above energy bands. The uncertainty of lags are estimated by Monte Carlo sim-

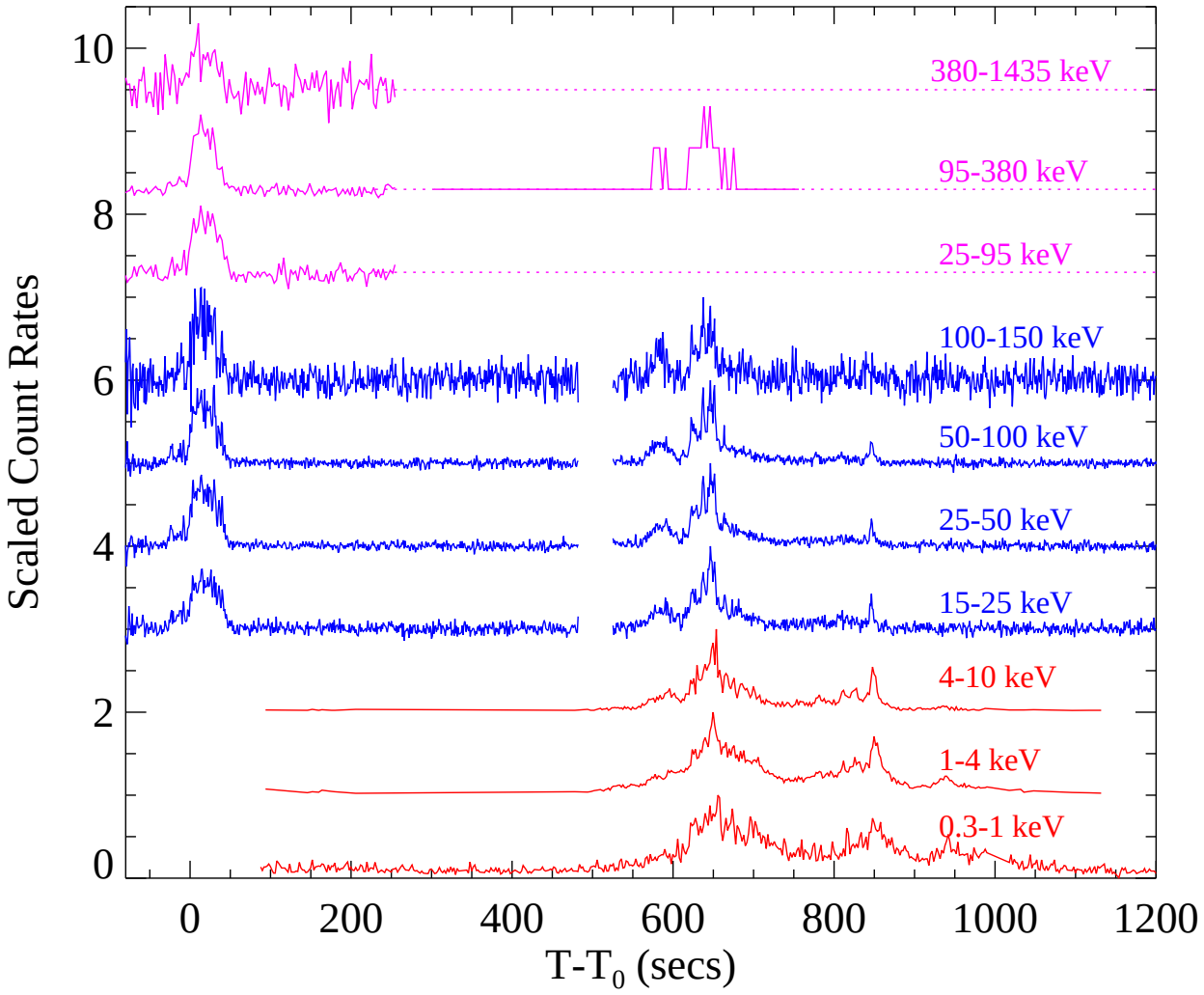

FIG. 5.— Multi-wavelength light curve for the prompt emission phase of GRB 110709B. Different color indicate different instruments as follows: *Magenta*: Konus-*WIND*; *blue*: *Swift*/BAT; *red*: *Swift*/XRT. The pulse width evolution with energy, namely the pulses in softer band tend to be broader, are similar with other GRBs (e.g., Romano et al 2006).

ulation (see e.g., Peterson et al.1998). We found that all those lags are consistent with zero. For the second sub-burst, we extracted 64ms-binned light curves in the same four BAT energy bands as mentioned above and three XRT energy bands: $0.3-1$ keV, $1-4$ keV and $4-10$ keV. Again, no significant lags were found between any two of those energy bands. In Fig 12, we plot the luminosity-lag diagram by assuming the double burst is at redshift $0.1-7.0$, where the upper limits of lags are defined as the temporal resolution (64 ms) of the light curves that we used to calculated lags. The zero lag for GRB 110709B is puzzling since it conflicts with the fact that it is a long burst, which in principle should exhibit spectral lags. One possible reason is that GRB 110709B might be a high redshift (i.e, z $\geq$ 2.0) burst with higher intrinsic luminosity so an intrinsic short lag is expected and might be undetectable. This is consistent with the non-detection of optical afterglow as described in §3.4

3.4. *A Dark Burst ?*

One puzzling feature of GRB 110709B is that there is no optical counterpart or host galaxy observed by UVOT or any other ground telescopes. Furthermore, no cataloged extragalactic galaxy was found within $1'$ radius in the NASA/IPAC Extragalactic Database (NED). Using the optical afterglow upper limits reported by Fong & Berger (2011), we plot the optical-to-X-ray SED at $T-T_0 = 3.2$ hours and $T-T_0$ =4.1 days in Fig. 13. The corresponding β_{OX} are > 0.75 and > 0.71 for the two epochs. Since bursts with $\beta_{OX} > -0.5$ are defined as "dark" (Jakobsson et al 2004, Greiner et al 2011), GRB 110709B is clearly an unusual dark burst with an extreme positive β_{OX}. Furthermore, the EVLA detection of radio counterpart of GRB 110709B gives further support that GRB 110709B is a dark burst (Zauderer & Berger 2011). The absence of the optical observation may indicate a high redshift origin (Fong & Berger 2011) or very different radiation mechanisms between the X-ray and optical components (D'Elia & Stratta, 2011).

4. IMPLICATIONS FOR THE CENTRAL ENGINE

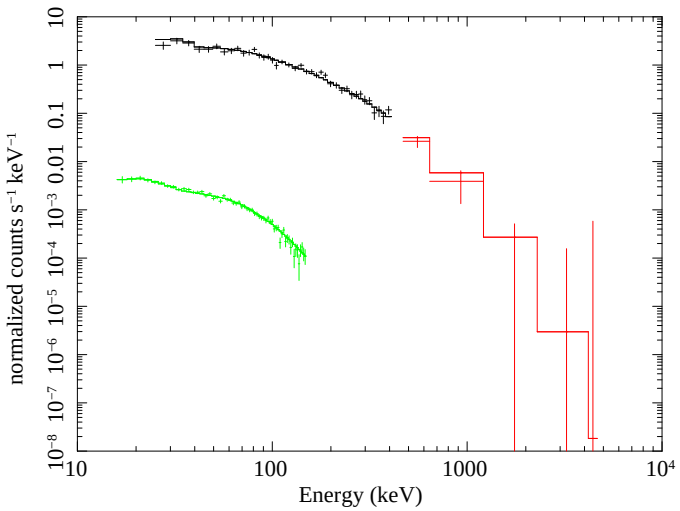

FIG. 6.— Joint fitting to time-averaged Konus-*WIND*+*Swift*/BAT spectra between 3.594-44.810 s. *Green*: *Swift*/BAT spectrum. *Black* and *red*: Konus-*WIND* spectra. Solid lines are the best-fit model.

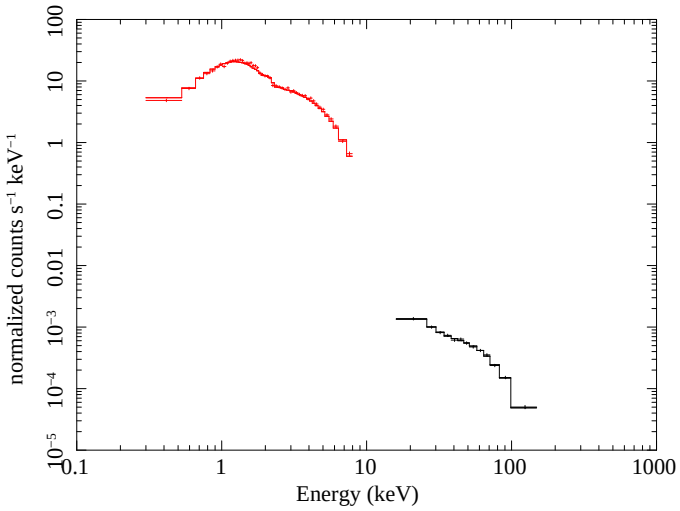

FIG. 7.— Joint fitting to time-averaged *Swift*/BAT+*Swift*/XRT spectra between 550-1000 s. *Red*: *Swift*/XRT spectrum. *Black*: *Swift*/BAT spectrum. Solid lines are the best-fit model.

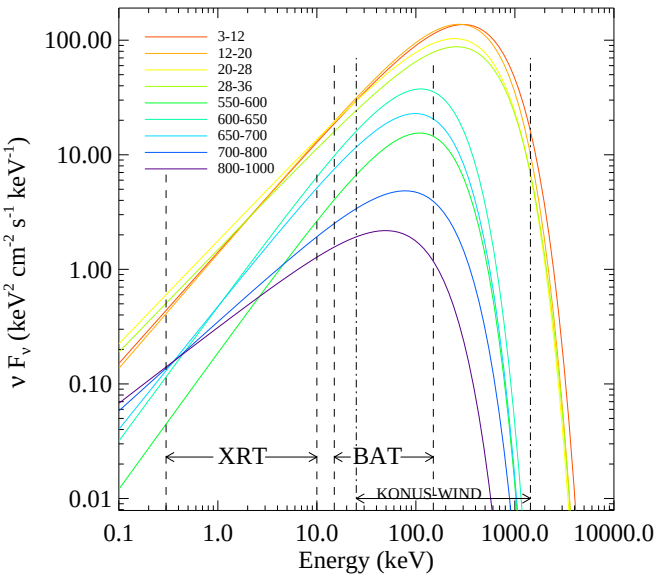

FIG. 8.— Modeled spectral energy distribution in different time intervals of the whole double burst period. Time intervals in seconds after T_0 are given in the legend.

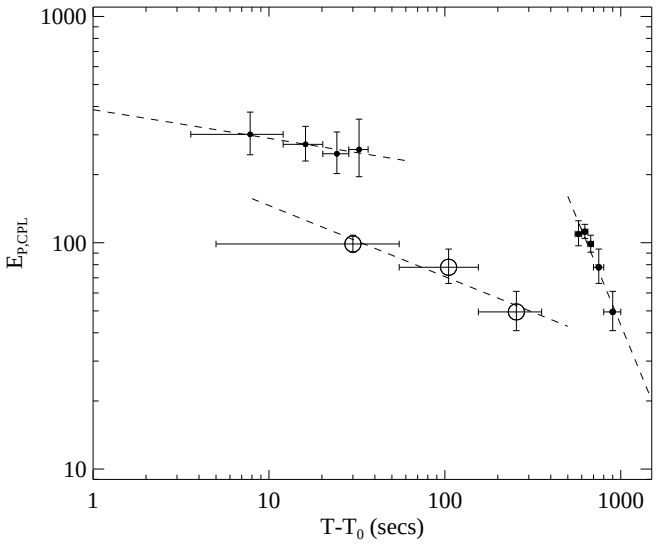

FIG. 9.— E_p as a function of time. Dashed lines indicate the simple power-law fit. For the first sub-burst (filled circles), $E_p \propto t^{-0.13}$ while for the second sub-burst (filled circles), $E_p \propto t^{-1.9}$. Open circles show the E_p evolution of the second sub-burst if T_0 is shifted to the trigger time of the second sub-burst, in which case $E_p \propto t^{-0.31}$.

Long-term central engine activities have been proved by the commonly detected X-ray flares which occur at hundreds of seconds after the burst trigger. This double burst GRB 110709B suggests that the long-term active central engine not only powers X-ray flares but also can power a second burst. Generally speaking, in order to produce a second "burst" as is observed in GRB 110709B, the central engine must restart with comparable or even larger energy. This is challenging for the following popular theoretical X-ray flare models:

- **Fragmentation in the massive star envelope.** The collapse of a rapidly rotating stellar core leads to fragmentation (King et al 2005). If the delayed accretion of fragmented debris leads a second burst, the debris must have comparable mass with the materials in the initial major accretion.
- **Fragmentation in the accretion disk.** Fragmentation in the accretion disk can power X-ray flares in both short and long GRBs (Perna et al 2006). In order to power a second burst instead of X-ray flares, the total mass of the fragmented outer part of the disk must be comparable to the initial disk mass.

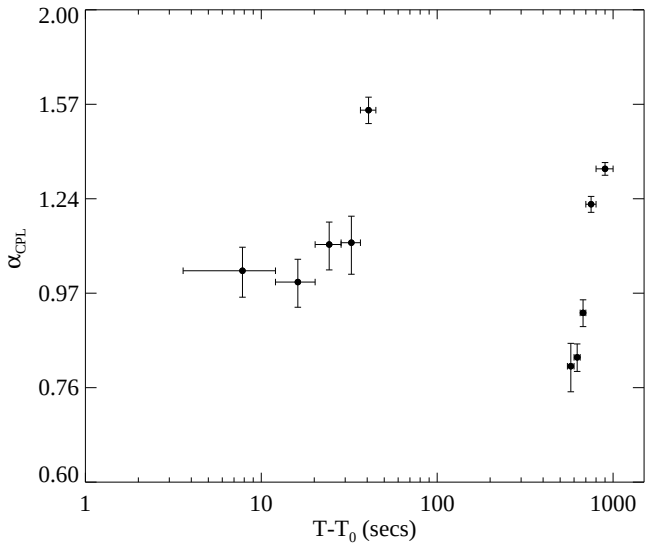

FIG. 10.— The spectral index of the cutoff power law model, α, as a function of time.

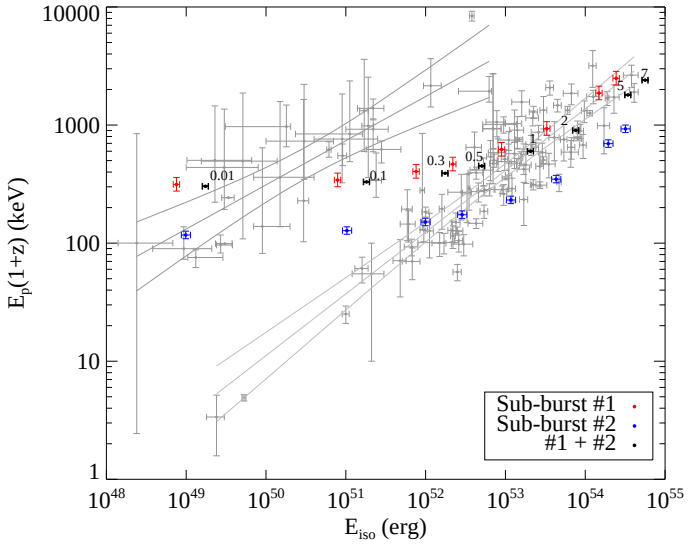

FIG. 11.— $E_p - E_{iso}$ plot made by putting the double burst at different assumed redshift z_x. *Red* : the first sub-burst. *Blue*: the second sub-burst. *Black*: the whole double burst. For each group of three points (red, blue and black), the nearest number indicates the corresponding assumed redshift z_x.

- **Magnetic barrier around the accretor.** Proga & Zhang (2006) argued that a magnetic barrier near the black hole may act as an effective modulator of the accretion flow. The delayed outflow can power the X-ray flares. This model, however is difficult to apply to the double burst mainly because it predicts that the late time accretion mass/rate is much lower and thus can not a power the gamma-ray energy.

On the other hand, the long quiescent gap between the two sub-bursts leads us to re-think the 2-stage fallback collapsar scenario that has been used to interpret GRB

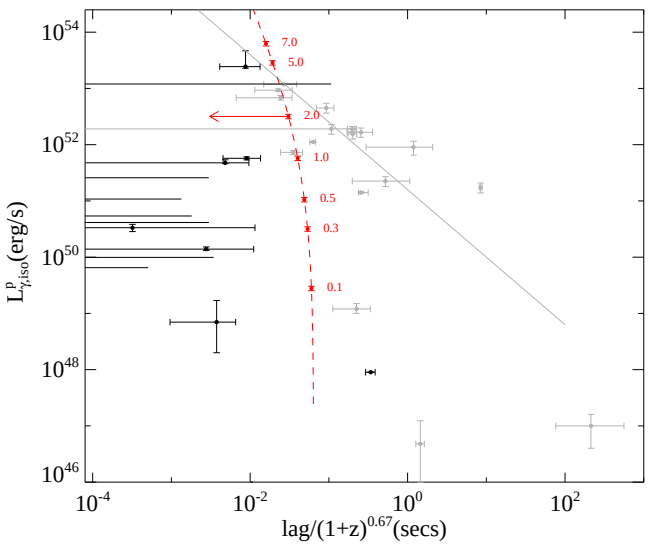

FIG. 12.— Luminosity-spectral lag diagram. Red points and dashed lines indicate the double burst's upper limits by for different assumed redshfit z_x. For clarity, no upper limit arrow is plotted except for z_x=2. Background grey data points are type II GRBs. Background back data points are type I and "other short-hard bursts" (Zhang et al 2009). The grey solid line represents the best linear fitting to type II bursts.

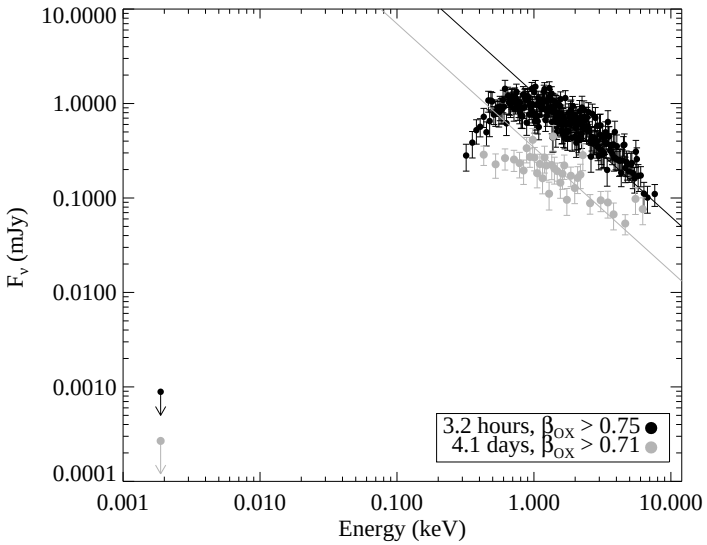

FIG. 13.— Optical to XRT band spectral energy distribution (SED) at $T - T_0 = 3.2$ hour and $T - T_0 = 4.1$ day. The R-band upper limits are obtained from Fong & Berger 2011. Solid lines are the power-law components fitted to XRT data only.

precursors (Wang & Mészáros, 2007). In that scenario, the precursor is produced by a weak jet formed during the initial core collapse, possibly related to MHD processes associated with a short-lived proto-neutron star, while the main burst is produced by a stronger jet fed by fallback accretion onto the black hole resulting from the collapse of the neutron star. We found that the assumed proto-neutron star rotational energy of few 10^{51} ergs in Wang & Mészáros, 2007 would also be sufficient, when

beaming is taken into account, to power the first sub-burst of GRB 110709B. In fact, simple estimates indicate that maximally rotating proto-neutron stars could reach rotational energies as high as several 10^{52} erg. Here, we propose a magnetar-to-BH scenario as follows:

(1) A magnetar is formed and produces the first sub-burst by releasing its rotation energy via electromagnetic and gravitational radiation in $\sim 10-20$ seconds (rest frame). A magnetar, rather than a lower field neutron star, is required not only to produce the high luminosity ($L_{\gamma,iso} \sim 10^{52}$ erg s^{-1}) and $E_{p,rest}$ ($\sim$ 0.6-1 MeV) of the first sub-burst (Zhang & Mészáros, 2001; Metzger et al. 2011), but also to overcome the ram pressure of the fallback matter (Wang & Mészáros, 2007). For a typical magnetar with proto-neutron star radius $R_{PNS} \sim 50$ km and mass $M_0 \sim 1.4 M_\odot$, the ram pressure can be written as $P_{\rm ram} = \frac{\dot{M} v_{ff}}{4\pi R_{PNS}^2} \simeq 5\times10^{26}\dot{M}_{-2}M_0^{1/2}\left(\frac{R_{PNS}}{50{\rm km}}\right)^{-5/2}{\rm erg\ s^{-1}}$, where $v_{ff} = (2GM/R_{PNS})^{1/2}$ is the free-fall velocity and $\dot{M}$ is the mass infalling rate in units of $M_\odot$ s^{-1} . The magnetic field pressure can be written as $P_B = B_f^2/8\pi \simeq 4\times10^{28}B_{f,15}^2$erg s^{-1}. Comparing the two, one can get $B_f \gtrsim 10^{14}$ G. Such a magnetized jet internally dissipates and powers the observed gamma-ray emission (e.g. Zhang & Yan 2011; Metzger et al. 2011).

(2) After the magnetar slows down, the magnetic outflow stresses decrease, so the ram pressure of the infalling matter becomes dominant. Thus the activity of the magnetar is suppressed during the accretion process. The accretion onto the magnetar does not lead to GRB emission, since the hot NS likely launches a dirty neutrino-driven wind with heavy baryon loading. In order to form a BH, a total accreting mass of 1 $M_\odot$ is needed. Assuming a redshift z=1, the accretion rate is about $\dot{M} \sim \frac{1M_\odot}{500s/(1+z)} \simeq 0.004 M_\odot/s$, which is consistent with theoretical predications in the supernova fallback scenario (see e.g., MacFadyen et al. 2001).

(3) The accretion finally leads the magnetar to collapse to a black hole. The second sub-burst is produced either from a baryonic or a magnetic jet. The spectrum will be softer either because the accretion leads the gas near the central engine to be more baryon-loaded so that the jet is slower or because the pre-existing channel from the first sub-burst may not have time to close so that the wide channel results in a slower jet and a softer spectrum. The spectral evolution of two stages would be expected to be different, since they are due to different physical process. These model features appear to be in concordance with the observed facts (see Fig 9).

5. CONCLUSION

GRB 110709B is the first GRB with two *Swift*/BAT triggers. Although separated by 11 minutes, the continuous spectral evolution of the two sub-bursts indicates that they may originate from the same central engine, which apparently requires extreme two-step activities that may be related to magnetar-to-BH accretion. On the other hand, we determined that GRB 110709B may be a high-z event according to its absence of optical observation together with the extreme β_{OX}, zero lags and (assumed) consistency to the Amati-relation.

We thank John Nousek, Judith L. Racusin, Peter Veres, Hao-Ning He, Eveline Helder, Jonathan Gelbord, En-Wei Liang, Suk Yee Yong and Fuwen Zhang for insightful comments that significantly improved the presentation of this paper. This work is partially supported by the following grants: NASA SAO SV4-74018 [BBZ], NASA NNX08AL40G [PM], NSF PHY-0757155 [PM], NSF AST-0908362 [BZ], NASA NNX10AD48G [BZ], ASI grants I/009/10/0 [GS], NSFC 10973008 [XYW] and the 973 program 2009CB824800 [XYW]. The Konus-Wind experiment is supported by the Russian Space Agency and the Russian Foundation for Basic Research (grants 09-02-00166 and 11-02-12082).

REFERENCES

Amati, L., Frontera, F., Tavani, M., et al. 2002, A&A, 390, 81
Aptekar, R. L., Frederiks, D. D., Golenetskii, S. V., et al. 1995, Space Sci. Rev., 71, 265
Barthelmy, S. D., Barbier, L. M., Cummings, J. R., et al. 2005, Space Sci. Rev., 120, 143
Barthelmy, S. D., Burrows, D. N., Cummings, J. R., et al. 2011, GRB Coordinates Network, 12124, 1
Beardmore, A. P., Evans, P. A., Goad, M. R., & Osborne, J. P. 2011, GRB Coordinates Network, 12136, 1
Burrows, D. N., Hill, J. E., Nousek, J. A., et al. 2005b, Space Sci. Rev., 120, 165
Burrows, D. N., Romano, P., Falcone, A., et al. 2005b, Science, 309, 1833
Cummings, J. R., Barthelmy, S. D., Burrows, D. N., et al. 2011a, GRB Coordinates Network, 12122, 1
Cummings, J. R., Barthelmy, S. D., Baumgartner, W. H., et al. 2011b, GRB Coordinates Network, 12144, 1
D'Elia, V., & Stratta, G. 2011, arXiv:1108.1054
D'Elia, V., Stratta, G., & Cummings, J. R. 2011, GRB Coordinates Network, 12142, 1
Eichler, D., Livio, M., Piran, T., & Schramm, D. N. 1989, Nature, 340, 126
Falcone, A. D., Morris, D., Racusin, J., et al. 2007, ApJ, 671, 1921
Falcone, A. D., Burrows, D. N., Lazzati, D., et al. 2006, ApJ, 641, 1010
Fan, Y. Z., & Wei, D. M. 2005, MNRAS, 364, L42
Fong, W., & Berger, E. 2011, GRB Coordinates Network, 12155, 1
Fryer, C. L. et al.
Golenetskii, S., Aptekar, R., Frederiks, D., et al. 2011, GRB Coordinates Network, 12135, 1
Greiner, J., Krühler, T., Klose, S., et al. 2011, A&A, 526, A30
Holland, S. T., & Cummings, J. R. 2011, GRB Coordinates Network, 12140, 1
Holland, S. T., & Cummings, J. R. 2011, GRB Coordinates Network, 12157, 1
Ioka, K., Kobayashi, S., & Zhang, B. 2005, ApJ, 631, 429
Jakobsson, P., Hjorth, J., Fynbo, J. P. U., et al. 2004, ApJ, 617, L21
King, A., O'Brien, P. T., Goad, M. R., et al. 2005, ApJ, 630, L113
Lazzati, D., & Perna, R. 2007, MNRAS, 375, L46
Liang, E.-W., Zhang, B.-B., Stamatikos, M., et al. 2006, ApJ, 653, L81
Liang, E.-W., Lü, H.-J., Hou, S.-J., Zhang, B.-B., & Zhang, B. 2009, ApJ, 707, 328
Liang, E.-W., Yi, S.-X., Zhang, J., et al. 2010, ApJ, 725, 2209
MacFadyen, A. I. & Woosley, S. E. 1999, ApJ, 524, 262
MacFadyen, A. I., Woosley, S. E., & Heger, A. 2001, ApJ, 550, 410
Mészáros, P. & Rees, M. J. 1997a, ApJ, 482, L29
Meszaros, P., & Rees, M. J. 1997b, ApJ, 476, 232
Metzger, B. D., Giannios, D., Thompson, T. A., Bucciantini, N., & Quataert, E. 2011, MNRAS, 413, 2031
Narayan, R., Paczynski, B., & Piran, T. 1992, ApJ, 395, L83
Paczýnski, B. 1986, ApJ, 308, L43
—. 1991, Acta Astronomica, 41, 257
Perna, R., Armitage, P. J., & Zhang, B. 2006, ApJ, 636, L29
Peterson, B. M., Wanders, I., Horne, K., et al. 1998, PASP, 110, 660

Proga, D., & Zhang, B. 2006, MNRAS, 370, L61
Rees, M. J. & Mészáros, P. 1994, ApJ, 430, L93
Romano, P., Moretti, A., Banat, P. L., et al. 2006, A&A, 450, 59
Romano, P., Campana, S., Chincarini, G., et al. 2006, A&A, 456, 917
Roming, P. W. A., Kennedy, T. E., Mason, K. O., et al. 2005, Space Sci. Rev., 120, 95
Sari, R., Piran, T., & Narayan, R. 1998, ApJ, 497, L17
Sari, R., & Piran, T. 1999, ApJ, 520, 641
Sari, R., & Piran, T. 1999, ApJ, 517, L109
Wang, X.-Y., & Mészáros, P. 2007, ApJ, 670, 1247
Woosley, S. E. 1993, ApJ, 405, 273
Wu, X. F., Dai, Z. G., Huang, Y. F., & Lu, T. 2005, ApJ, 619, 968
Yamazaki, R. 2009, ApJ, 690, L118
Zauderer, A., & Berger, E. 2011, GRB Coordinates Network, 12190, 1
Zhang, B. 2007, ChJAA, 7, 1
Zhang, B., & Mészáros, P. 2001, ApJ, 552, L35
Zhang, B., Yan, H., 2011, ApJ, 726, 90
Zhang, B., Zhang, B.-B., Virgili, F. J., et al. 2009, ApJ, 703, 1696
Zhang, B.-B., Liang, E.-W., & Zhang, B. 2007, ApJ, 666, 1002